

Relief of frustration through spin disorder in multiferroic $\text{Ho}_{1-x}\text{Y}_x\text{MnO}_3$

H. D. Zhou,^{1,2,*} J. Lu,² R. Vasic,^{1,2} B. W. Vogt,² J. A. Janik,² J. S. Brooks,^{1,2} and C. R. Wiebe^{1,2}

¹Department of Physics, Florida State University, Tallahassee, Florida 32306-3016, USA

²National High Magnetic Field Laboratory, Florida State University, Tallahassee, Florida 32306-4005, USA

(Received 9 February 2007; revised manuscript received 16 March 2007; published 23 April 2007)

The magnetic phase diagram of single crystalline $\text{Ho}_{1-x}\text{Y}_x\text{MnO}_3$ below T_N is determined by measuring the magnetic susceptibility (χ), specific heat (C_p), dielectric constant (ϵ), and thermal conductivity (κ). Y doping enhances the $P6_3cm$ magnetic phase below T_{SR} and therefore increases T_{SR} ; only the $P6_3cm$ phase exists below T_N for $x \geq 0.9$ samples. Y doping also reduces the $P6_3cm$ phase below T_2 . The anomaly around T_{SR} appears in the dielectric constant but is absent in χ and C_p for $\text{Ho}_{0.3}\text{Y}_{0.7}\text{MnO}_3$ and $\text{Ho}_{0.2}\text{Y}_{0.8}\text{MnO}_3$ samples, which indicates that the multiferroicity at T_{SR} for HoMnO_3 is not necessarily related to the Ho^{3+} spin ordering. Specific heat measurements show that the large electronic specific heat (γ) of HoMnO_3 is related to the disorder of Ho^{3+} spins, and is correlated with the relief of frustration in the Mn sublattice. The thermal conductivity data support an enhanced spin-lattice interaction due to strong spin fluctuations in the geometrically frustrated Mn-spin system.

DOI: 10.1103/PhysRevB.75.132406

PACS number(s): 75.47.Lx, 75.30.Kz, 65.40.Ba

The RMnO_3 compounds with hexagonal structure (R represents from Ho to Lu and Y) have attracted considerable recent attention because of the coupling between ferroelectricity and antiferromagnetic order, and also the geometrically frustrated dominant spin-spin interactions between Mn^{3+} ions within the close-packed basal planes.¹⁻⁹ With different rare earth elements on the A site, RMnO_3 shows different magnetic symmetry and physical properties below T_N . HoMnO_3 and YMnO_3 are two examples of systems with very different ground states. For HoMnO_3 : (i) below $T_N \approx 70$ K, the magnetic symmetry changes from $P6_3cm$ to $P6_3cm$ at $T_{SR} = 33$ K or 40 K (Refs. 10 and 11) with a 90° rotation of the Mn spins. The symmetry then changes to $P6_3cm$ at $T_2 \approx 5$ K with another 90° rotation of the Mn spins, which is accompanied by a magnetic ordering of the Ho^{3+} -ion spins orientated along the c axis;¹² (ii) the frustration factor $f = \theta_{CW}/T_N \approx 1$;¹³ and (iii) the specific heat data give an unusual large electronic contribution with $\gamma = 0.19$ J/mol K².¹⁴ For YMnO_3 , the magnetic symmetry is $P6_3cm$ below $T_N \approx 70$ K, $f \approx 8$,¹⁵ and γ is near zero. The goal of this work is to explain the origin of the linear component of the specific heat through systematic doping with nonmagnetic Y. This feature is anomalous. We show evidence of an enhanced specific heat based upon Ho spin disorder, which is correlated with a change in the frustration index, and with increased thermal conductivity at low temperatures. We also clarify some features in the Y-doping phase diagram.

Single crystals of $\text{Ho}_{1-x}\text{Y}_x\text{MnO}_3$ ($0 \leq x \leq 1.0$) were grown by the traveling-solvent floating-zone technique. All samples were single-phase with the hexagonal $P6_3cm$ structure via powder x-ray diffraction. With increasing x , the lattice parameter a decreases and c increases linearly. X-ray Laue diffraction was used to orient the crystal. The magnetic-susceptibility measurements were made with a Quantum Design dc superconducting interference device magnetometer with an applied field of 100 Oe along the c axis; the measurements were made on heating after cooling in zero field. The specific heat measurements were performed on a

PPMS (Physical Property Measurement System, Quantum Design) at temperatures from 2 to 100 K. The thermal conductivity $\kappa(T)$ was measured along the c axis in the temperature region 7–300 K with a steady-state heat-flow technique. A standard ac capacitance bridge method was used to measure the real (capacitive, C) and loss (dissipative, D) signals at 100 KHz with parallel plate silver electrodes normal to the c axis.

Figure 1 shows the temperature dependences of $d(1/\chi)/dT$ for $\text{Ho}_{1-x}\text{Y}_x\text{MnO}_3$ over the temperature range $25 \text{ K} < T < 65 \text{ K}$ and $1.8 \text{ K} < T < 7 \text{ K}$. The derivatives show peaks at T_{SR} and T_2 , which are 40 K and 5 K, respectively, for HoMnO_3 . With increasing x , T_{SR} increases and T_2 decreases.

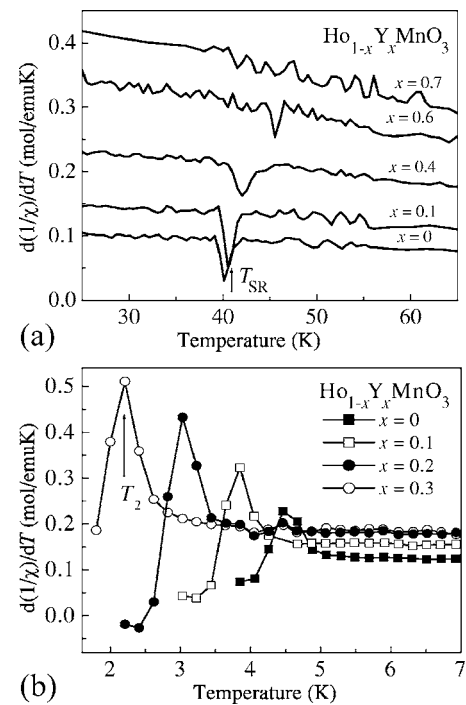


FIG. 1. Temperature dependences of $d(1/\chi)/dT$ with $25 \text{ K} < T < 65 \text{ K}$ (a) and $1.8 \text{ K} < T < 7 \text{ K}$ (b) for $\text{Ho}_{1-x}\text{Y}_x\text{MnO}_3$.

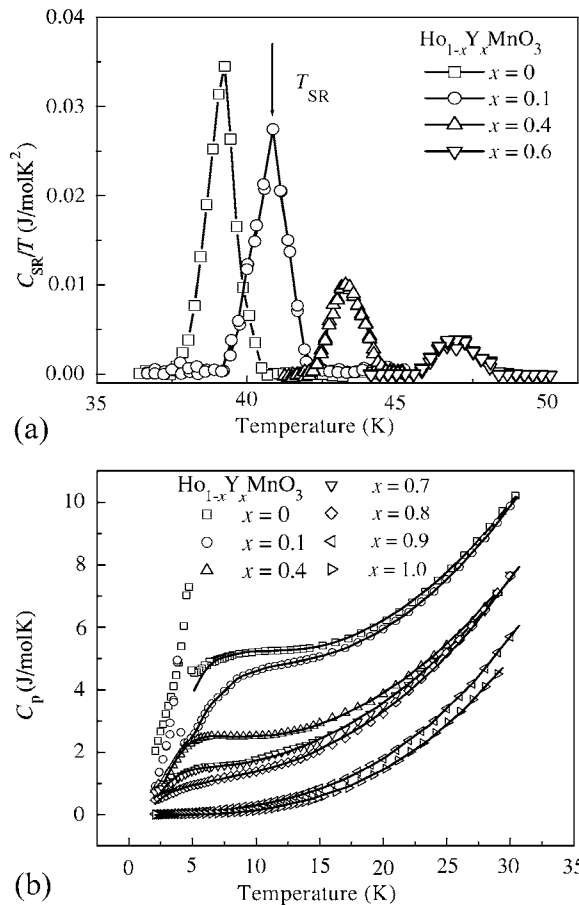


FIG. 2. Temperature dependences of specific heat C_p around T_{SR} (a) and with $2 < T < 30$ K (b) for $\text{Ho}_{1-x}\text{Y}_x\text{MnO}_3$. The solid lines are fittings using Eq. (1).

For samples with $x > 0.6$, no such peak at T_{SR} is observed by susceptibility measurements.

The specific heat data of $\text{Ho}_{1-x}\text{Y}_x\text{MnO}_3$ show three anomalies: (i) a λ -type anomaly at T_N , not shown here; (ii) a narrow peak around T_{SR} , Fig. 2(a), which is plotted as C_{SR}/T (C_{SR}/T is obtained by subtracting a linear background fit from C_p/T in a small temperature range near T_{SR}); and (iii) a sharp peak at T_2 , Fig. 2(b). With increasing x , (i) T_N remains around 70 K, which is also confirmed by the thermal conductivity measurements, Fig. 3; (ii) with Y doping, the inten-

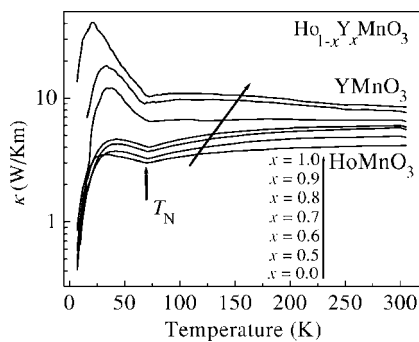


FIG. 3. Temperature dependences of thermal conductivity for $\text{Ho}_{1-x}\text{Y}_x\text{MnO}_3$.

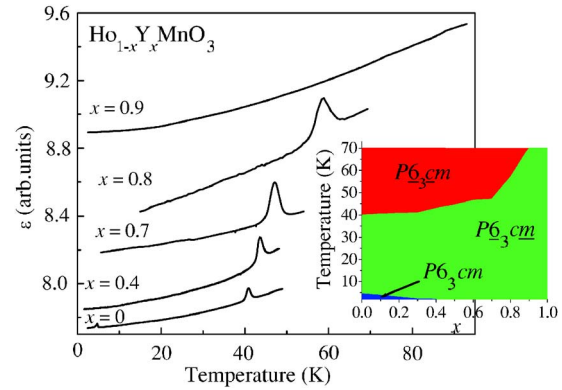


FIG. 4. (Color online) Temperature dependences of dielectric constant ϵ for $\text{Ho}_{1-x}\text{Y}_x\text{MnO}_3$; inset, the magnetic phase diagrams below 70 K for $\text{Ho}_{1-x}\text{Y}_x\text{MnO}_3$.

sity of the peak around T_{SR} decreases but the value of T_{SR} increases; with $x > 0.6$ no peak at T_{SR} is observed from specific heat below T_N ; (iii) both the intensity of the peak around T_2 and the value of T_2 decrease as a function of doping; and (iv) the broad peak between 5 K and 10 K for HoMnO_3 gradually moves to low temperatures and disappears with Y doping.

Two features are noteworthy from the thermal conductivity data (Fig. 3): (i) at temperatures $T > T_N$, $\kappa(T)$ shows a relatively weak temperature dependence. With increasing x , the magnitude of the thermal conductivity increases; and (ii) $\kappa(T)$ undergoes an increase at the onset of antiferromagnetic order below T_N ; and with increasing x , T_N remains unchanged.

The dielectric constant data of $\text{Ho}_{1-x}\text{Y}_x\text{MnO}_3$, Fig. 4, shows sharp peaks around T_{SR} and T_2 . The values of T_{SR} and T_2 obtained here are consistent with those obtained from susceptibility and specific heat measurements. One outstanding feature is that although no peak around T_{SR} is observed from the susceptibility and specific heat measurements for samples with $x > 0.6$, the dielectric constants show a peak for $x = 0.7$ and $x = 0.8$ samples at 47 K and 58 K, respectively, which indicates that the T_{SR} keeps increasing with increasing x . For the $x = 0.9$ sample, the dielectric constant shows no peak below 70 K.

The magnetic phase diagram below 70 K for $\text{Ho}_{1-x}\text{Y}_x\text{MnO}_3$ determined by T_{SR} and T_2 is shown in Fig. 4 (inset). It is clear that Y doping favors the formation of the $P6_3cm$ magnetic phase below T_{SR} and increases T_{SR} . The $P6_3cm$ phase occupies the whole temperature region below T_N for $x \geq 0.9$ samples, so there is no T_{SR} for the transition from the $P6_3cm$ to the $P6_3cm$ phase, and accordingly there is no peak for the dielectric constant. Y doping also dilutes the Ho-O-Ho interactions, so T_2 decreases with increasing x . These results show that the multiferroicity of HoMnO_3 is tunable by changing the volume fractions of the different magnetic phases below T_N .

The observed peaks for the specific heat and susceptibility at T_{SR} are due to the partial Ho^{3+} spin ordering, which have also been inferred from dc susceptibility and neutron scattering data.¹⁶⁻¹⁸ The reorientation of Mn spins is strictly confined in the ab plane. It cannot account for the entropy

TABLE I. Parameters obtained from the fit of experimental specific heat data to Eq. (1) for $\text{Ho}_{1-x}\text{Y}_x\text{MnO}_3$.

x	γ (J/mol K ²)	β (10 ⁻⁴ J/mol K ⁴)	A	Δ_1 (K)	Δ_2 (K)
0	0.19(1)	1.3(2)	1.0	17.8(2)	35.6(2)
0.1	0.17(1)	1.5(1)	0.91(1)	15.0(1)	33.0(1)
0.4	0.14(1)	1.5(2)	0.80(3)	12.2(2)	26.0(2)
0.7	0.10(2)	1.6(2)	0.71(2)	10.5(2)	21.8(2)
0.8	0.09(1)	1.8(2)	0.65(1)	9.0(1)	19.7(1)
0.9	0.01(1)	1.8(2)			
1.0	0	1.8(2)			

change and the c -axis susceptibility change. The disappearance of peaks for $x > 0.6$ samples from specific heat and susceptibility suggests that the Y doping almost destroys this ordering. At the same time, the dielectric constant still shows a peak around T_{SR} for $x=0.7$ and 0.8 samples. This difference indicates that the multiferroicity at T_{SR} for HoMnO_3 is not necessary related to the Ho^{3+} spin ordering.

The broad peak of C_p at low temperature which gradually disappears with increasing x in $\text{Ho}_{1-x}\text{Y}_x\text{MnO}_3$ could be explained as a Schottky anomaly related to the Ho^{3+} ion.¹⁴ Thus, for $T \ll \theta_D$, we may describe C_p as

$$C_p = C_e + C_{\text{ph}} + C_{\text{sch}}, \quad (1)$$

with

$$C_e = \gamma T, \quad (2)$$

$$C_{\text{ph}} = \beta T^3, \quad (3)$$

$$C_{\text{sch}} = A(1-x) \frac{R}{T^2} \left\{ \frac{\sum_{i=1}^n \Delta_i^2 \exp\left(\frac{-\Delta_i}{T}\right)}{\sum_{i=1}^n \exp\left(\frac{-\Delta_i}{T}\right)} - \left[\frac{\sum_{i=1}^n \Delta_i \exp\left(\frac{-\Delta_i}{T}\right)}{\sum_{i=1}^n \exp\left(\frac{-\Delta_i}{T}\right)} \right]^2 \right\}. \quad (4)$$

These terms correspond to contributions from electrons, phonons, and Schottky anomalies, respectively. Here, $\beta = N(12/5)\pi^4 R \theta_D^3$ with $N=5$ as the number of atoms in the unit cell and $R=8.314$ J/mol K as the ideal gas constant; A is a constant which specifies the percentage of the number of Ho^{3+} ions per formula unit involved with the Schottky anomaly; x is the Y-doping percentage; and Δ_i is the i th energy level of the crystal field in Kelvin.^{19,20} For our temperature range, we choose $i=2$ based upon the recent neutron scattering data,²¹ which indicates there are two crystal field levels of Ho at 1.5 meV (17.4 K) and 3.1 meV (36 K). The solid curves shown in Fig. 2(b) are fits of experimental data (open circles) and the fitting parameters are listed in Table I. Several features are noteworthy from the extracted parameters: (i) Δ_1 and Δ_2 derived from the fit are 17.8(2) K and 35.6(2) K for HoMnO_3 , which are consistent with the 17.4 K and 36 K obtained from the neutron scattering experiment; and (ii) γ decreases linearly with increasing x until

$x=0.8$, and then suddenly drops to near zero for $x=0.9$ and 1.0 samples, Fig. 5. The magnitude of γ (0.19–0.10 J/mol K²) for samples with $x \leq 0.8$ is about two orders of magnitude larger than the values observed from typical free electron terms, which is unusual for electrical insulators such as $\text{Ho}_{1-x}\text{Y}_x\text{MnO}_3$. The decrease of γ with Y doping clearly shows that the large γ is related to the disorder of Ho^{3+} spins above the ordering temperature T_2 , which has been shown as a slow increase of the Ho magnetic Bragg peaks' intensity between 32 K and 5 K from the neutron scattering data.¹⁸ The appearance of this linear term can be explained as due to the high degeneracy of disordered Ho^{3+} spins above the 5 K ordering temperature.^{22,23} The sudden drop of the value of γ to nearly zero for the $x=0.9$ and 1.0 samples is correlated with the phase diagram in Fig. 3, and shows that the $P6_3cm$ phase from YMnO_3 has occupied the whole temperature region below T_N and dominated the magnetic behavior. We also calculated the frustration factor $f = \theta_{\text{CW}}/T_N$ to compare with the change in the linear specific heat term. As shown in Fig. 5, f increases slowly with increasing x until $x=0.8$, and then jumps to large high values for the $x=0.9$ and 1.0 samples. This result further confirms that with $x \geq 0.9$, the $P6_3cm$ phase already dominated the magnetic behavior. It also indicates that doping with Ho^{3+} spins relieves the frustration of the YMnO_3 system. (iii) The decrease of the A and Δ values with increasing x reflects that the number of Ho^{3+} ions involved for Schottky anomaly and the splitting of the energy levels both decrease with the dilution of Ho-O-Ho interactions.

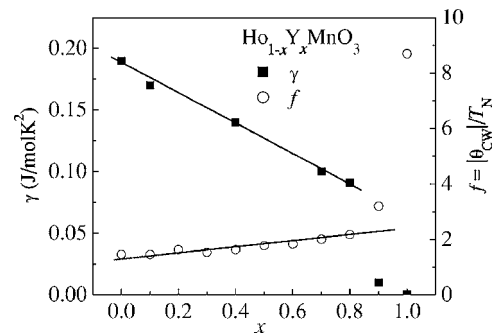


FIG. 5. Variation with x of γ and f for $\text{Ho}_{1-x}\text{Y}_x\text{MnO}_3$.

Above T_N , the thermal conductivity $\kappa(T)$ should be dominated by the phonon contribution described by the Debye model²⁴ and approach a $1/T$ law at high temperatures (usually for $T > \theta_D/4$). The nearly temperature-independent $\kappa(T)$ for $\text{Ho}_{1-x}\text{Y}_x\text{MnO}_3$ deviates from the $1/T$ law. This is reminiscent of enhanced thermal conductivity due to phonon-spin excitation scattering.²⁵ The peak at low temperatures increases by an order of magnitude from HoMnO_3 to YMnO_3 , and is thus an indicator of enhanced spin fluctuations in the highly frustrated YMnO_3 sublattice (which has a high frustration parameter f).¹¹ The enhanced spin fluctuations in YMnO_3 are apparent via neutron scattering measurements, which have noted a rich excitation spectrum with a two-dimensional Kosterlitz-Thouless character.²⁶ The suppression of the thermal conductivity is connected with an increase in the linear specific heat coefficient and a drop in the frustration index as the Ho doping relieves the frustration in the Mn sublattice through magnetic defects. This is another example of the “order by disorder” mechanism in frustrated systems, where a system chooses an ordered state out of the nearly degenerate number of states through the breaking of symmetry.²⁷ In this case, the transitional symmetry of the lattice is broken with the addition of random Ho^{3+} spins.

Based on the present studies of $\text{Ho}_{1-x}\text{Y}_x\text{MnO}_3$, it has been demonstrated that (i) Y doping increases T_{SR} by enhancing $P6_3cm$ magnetic phase below T_{SR} . Only the $P6_3cm$ phase exists below T_N for $x \geq 0.9$ samples. Y doping also dilutes the Ho-O-Ho interactions to diminish the $P6_3cm$ phase below T_2 ; (ii) the multiferrocity at T_{SR} for HoMnO_3 is not necessary related to the Ho^{3+} spin ordering; (iii) the large γ of HoMnO_3 is related to the disorder of Ho^{3+} spins above the ordering temperature T_2 , and the number of Ho^{3+} ions involved for Schottky anomaly and the splitting of the energy levels both decrease with increasing Y doping; and (iv) doping with Ho^{3+} magnetic moments suppresses the thermal conductivity due to the relief of frustration in the YMnO_3 sublattice, and a corresponding change in the spin dynamics.

This work was supported by a contractual agreement between the NSF and the State of Florida through NHMFL. A portion of this work was performed by NSF Cooperative Contract No. DMR-0084173, by the State of Florida, and by the DOE. Additional support was through Grant No. NSF-DMR 0602859. The authors would also like to acknowledge the support of Florida State University through the EIEG program.

*Electronic address: zhou@magnet.fsu.edu

- ¹B. B. Van Aken, T. T. M. Palstra, A. Filippetti, and N. A. Spaldin, *Nat. Mater.* **3**, 164 (2004).
- ²M. Fiebig, D. Fröhlich, K. Kohn, St. Leute, Th. Lottermoser, V. V. Pavlov, and R. V. Pisarev, *Phys. Rev. Lett.* **84**, 5620 (2000).
- ³Seongsu Lee, A. Pirogov, Jung Hoon Han, J.-G. Park, A. Hoshikawa, and T. Kamiyama, *Phys. Rev. B* **71**, 180413(R) (2005).
- ⁴B. Lorenz, A. P. Litvinchuk, M. M. Gospodinov, and C. W. Chu, *Phys. Rev. Lett.* **92**, 087204 (2004).
- ⁵C. dela Cruz, F. Yen, B. Lorenz, Y. Q. Wang, Y. Y. Sun, M. M. Gospodinov, and C. W. Chu, *Phys. Rev. B* **71**, 060407(R) (2005).
- ⁶U. Adem, A. A. Nugroho, A. Meetsma, and T. T. M. Palstra, *Phys. Rev. B* **75**, 014108 (2007).
- ⁷R. Vasic, H. D. Zhou, E. Jobilong, C. R. Wiebe, and J. S. Brooks, *Phys. Rev. B* **75**, 014436 (2007).
- ⁸V. Laukhin, V. Skumryev, X. Martí, D. Hrabovsky, F. Sánchez, M. V. García-Cuenca, C. Ferrater, M. Varela, U. Lüders, J. F. Bobo, and J. Fontcuberta, *Phys. Rev. Lett.* **97**, 227201 (2006).
- ⁹M. Tachibana, J. Yamazaki, H. Kawaji, and T. Atake, *Phys. Rev. B* **72**, 064434 (2005).
- ¹⁰F. Yen, C. R. dela Cruz, B. Lorenz, Y. Y. Sun, Y. Q. Wang, M. M. Gospodinov, and C. W. Chu, *Phys. Rev. B* **71**, 180407(R) (2005).
- ¹¹H. D. Zhou, J. C. Denyszyn, and J. B. Goodenough, *Phys. Rev. B* **72**, 224401 (2005).
- ¹²M. Fiebig, T. Lottermoser, D. Fröhlich, A. V. Goitsev, and R. V. Pisarev, *Nature (London)* **419**, 818 (2002).
- ¹³H. Sugie, N. Iwata, and K. Kohn, *J. Phys. Soc. Jpn.* **71**, 1558 (2001).
- ¹⁴H. D. Zhou, J. A. Janik, B. W. Vogt, Y. J. Jo, L. Balicas, M. J. Case, C. R. Wiebe, J. C. Denyszyn, J. B. Goodenough, and J. G. Cheng, *Phys. Rev. B* **74**, 094426 (2006).
- ¹⁵T. Katsufuji, S. Mori, M. Masaki, Y. Moritomo, N. Yamamoto, and H. Takagi, *Phys. Rev. B* **64**, 104419 (2001).
- ¹⁶B. Lorenz, F. Yen, M. M. Gospodinov, and C. W. Chu, *Phys. Rev. B* **71**, 014438 (2005).
- ¹⁷A. Muñoz, J. A. Alonso, M. J. Martínez-lope, M. T. Casáis, J. L. Martínez, and M. T. Fernández-Díaz, *Chem. Mater.* **13**, 1497 (2001).
- ¹⁸Th. Lonkai, D. Hohlwein, J. Ihringer, and W. Prandl, *Appl. Phys. A: Mater. Sci. Process.* **74**, 843 (2002).
- ¹⁹Y. M. Jana, O. Sakai, R. Higashinaka, H. Fukazawa, Y. Maeno, P. Dasgupta, and D. Ghosh, *Phys. Rev. B* **68**, 174413 (2003).
- ²⁰V. Sima, M. Davis, P. Svoboda, Z. Smetana, S. Zajac, and J. Bischoff, *J. Phys.: Condens. Matter* **1**, 10153 (1989).
- ²¹O. P. Vajk, M. Kenzelmann, J. W. Lynn, S. B. Kim, and S. W. Cheong, *Phys. Rev. Lett.* **94**, 087601 (2005).
- ²²P. Raychaudhuri, C. Mitra, A. Paramekanti, R. Pinto, A. K. Nigma, and S. K. Dhar, *J. Phys.: Condens. Matter* **10**, L191 (1998).
- ²³L. Ghivelder, I. A. Castillo, M. A. Gusmão, J. A. Alonso, and L. F. Cohen, *Phys. Rev. B* **60**, 12184 (1999).
- ²⁴R. Berman, *Thermal Conduction in Solids* (Clarendon, Oxford, 1976).
- ²⁵Y. Ando, J. Takeya, D. L. Sisson, S. G. Doettinger, I. Tanaka, R. S. Feigelson, and A. Kapitulnik, *Phys. Rev. B* **58**, R2913 (1998).
- ²⁶T. J. Sato, S.-H. Lee, T. Katsufuji, M. Masaki, S. Park, J. R. D. Copley, and H. Takagi, *Phys. Rev. B* **68**, 014432 (2003).
- ²⁷J. N. Reimers and A. J. Berlinsky, *Phys. Rev. B* **48**, 9539 (1993).